Physics of Wind Energy: Final Project Report

Robert Spragg, Paul Yi, Gabriel Buchsbaum

March 13, 2018

Abstract

Wind data from a site in Texas is used to study and quantify how varying the turbine hub heights under various incoming wind conditions affects the capacity factor and reliability of a wind farm. Using six years of wind measurements from four heights, a suite of power law velocity profiles are generated. These profiles attempt to capture the variability of the incoming winds at the site of interest. A sensitivity analysis of varying the wind profile parameters is carried out to estimate the optimal hub height placement for specific wind conditions.
Keywords: Optimization, Wake effects, Hellman exponent, Velocity deficit

1 Introduction

The majority of modern wind farms have a standardized rotor height and blade size. This has traditionally occurred for the sake of simplicity, as uniform projects are easier to finance and construct. Allowing for flexible rotor heights, however, may enable increased capacity factors and reduced structural loading, whose benefits may outweigh the costs associated with added project complexity. This report aims to develop an algorithm that calculates the optimal hub height variations for a wind farm, given its unique wind parameters and terrain geometry. The report will only consider a prescribed set of locations for the turbines; an algorithm that provides the optimal siting of each turbine is a topic for future research.

1.1 Literature Review

An experimental study by Vested et al. (2014) considered the power output of four different farm arrangements involving tall and short turbines. Using wind tunnel measurements, the power output of these four arrangements with variable turbine hub heights were compared to the base case involving the short turbines only. The tall turbines had a set hub height of $1.5 * h_{\text{small}}$. Their configuration and results are summarized below in Figures 1 and 2.

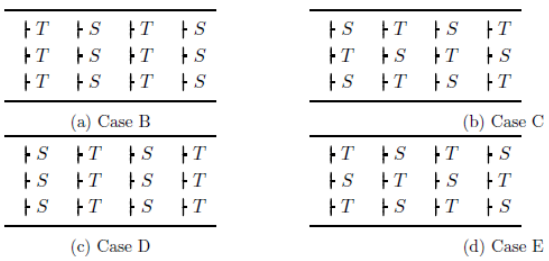

Figure 1: Four wind turbine arrangements from Vested et al. (2014). Cases B and D exhibit row-by-row variations, while Cases C and E exhibit checkerboard variations.

When total power was considered, there were very different results depending on the given arrangement, as shown below in Figure 2.

Table 1: Power for each turbine based on the particular case.

Configuration	Row 1	Row 2	Row 3	Row 4	Total
A $(S-S-S-S)$	0.14	0.08	0.08	0.08	0.38
B $(T-S-T-S)$	0.20	0.11	0.10	0.10	0.51
D $(S-T-S-T)$	0.14	0.14	0.10	0.10	0.48
E $(S-T-S-T)$	0.14	0.12	0.09	0.11	0.46

Figure 2: Note the power differences between cases B, D, and E

Bastankhah and Porté-Agel (2014) presented a Gaussian velocity deficit expression for the wake of a single wind turbine. Subsequently, the study by Niayifar and Porté-Agel (2016) extended this model to estimate the power generated in a wind farm and tested the analytical predictions against large eddy simulation (LES) model results. The equation for a normalized velocity deficit with a Gaussian shape is

$$\frac{\Delta U}{U_\infty} = \left(1 - \sqrt{1 - \frac{C_T}{8(k_w x/d_0 + \epsilon)^2}}\right) \times \exp\left(-\frac{1}{2(k_w x/d_0 + \epsilon)^2}\left\{\left(\frac{z - z_h}{d_0}\right)^2 + \left(\frac{y}{d_0}\right)^2\right\}\right). \tag{1}$$

In Equation (1), ΔU is the velocity deficit at a given point (x, y, z) behind the turbine, U_∞ is the free-stream velocity of the wind farm, z_h is the turbine hub height, and k_w is the wake growth rate. The wake growth rate (k_w) is a function of the thrust coefficient (C_T) and turbulence intensity.

In class, Professor Dabiri described a simple, power law profile for estimating the wind profile at a site:

$$u(z) = u(z_r) \times \left(\frac{z}{z_r}\right)^a, \tag{2}$$

where $u(z_r)$ is the wind speed at the reference height, and a is the Hellman exponent. Typical values for the Hellman exponent are on the order of $\frac{1}{7}$. We will estimate incoming velocities using Eq. (2).

2 Motivation

Currently, predicting the power output from wind farms has a large error bound compared to solar technology (PV). The following chart, from Fitch Ratings, (Figure 3) highlights this discrepancy.

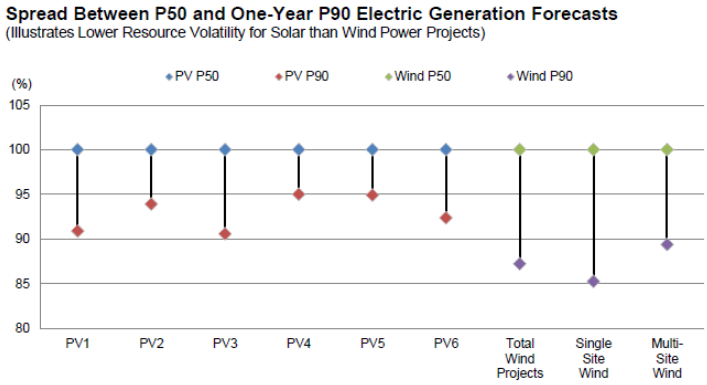

Figure 3: The P50 is the amount of power that will be generated during 50% or more of the operating years. The P90 is the amount that will be generated during 90% or more of the operating years. A larger spread means more uncertainty and thus more financial risk.

Furthermore, wind energy predictions have overestimated generation at many sites, putting developers and lenders in a bind. While predictions have become more accurate during the past few years, there is still room for improvement. If uncertainties associated with calculating the capacity factor can be reduced by turbine arrays with varying hub heights, one might be able to not only improve the wind farm's capacity factor, but also create more accurate predictions of annual energy output.

3 Approach

This paper uses (a) a turbine arrangement similar to that in Vested et al. (2014), combined with (b) the wake model described in Bastankhah and Porté-Agel, as well as (c) the power law profile for $u(z)$ described by Professor Dabiri, as inputs into an optimization model in the Julia programming language. The Julia model then outputs the optimal hub height for each turbine as well as the total power output for the optimal turbine arrangement.

To calculate the variations in velocity with height, the wind statistics for a site of interest must be developed. Our team has leveraged data from MAP Royalty, Inc. to develop our inflow velocity profile $u(z)$. The dataset contains 6 years of 10-minute averaged wind speed data for multiple heights from a MET tower in the Texas Panhandle. The wind resource for each season is shown below in Figures 4 and 5. In spring, summer, and autumn, the prevailing wind is out of the west.

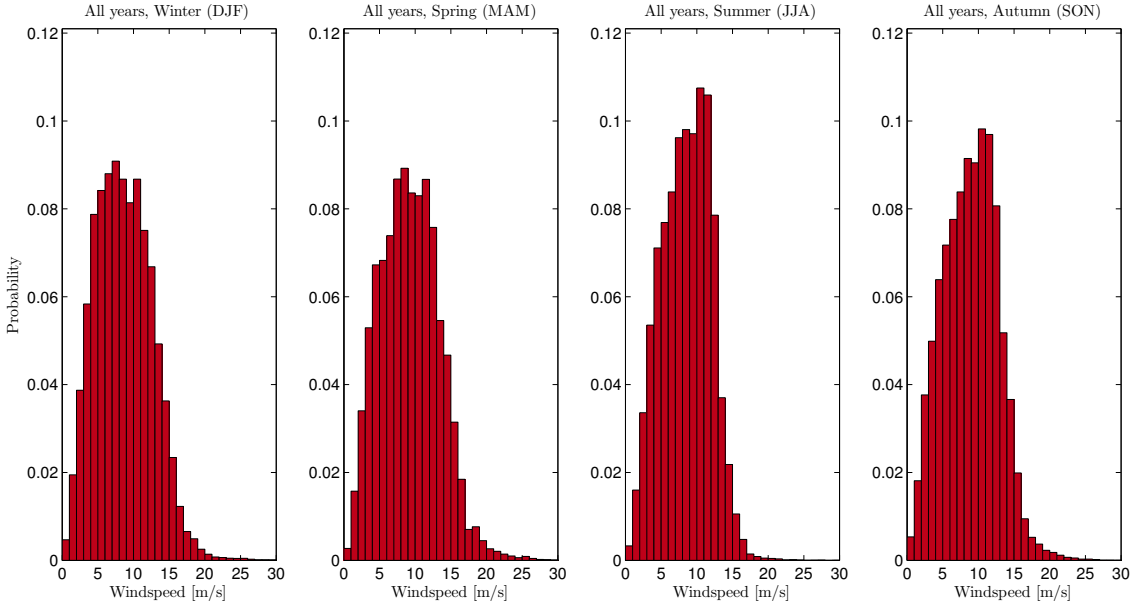

Figure 4: Wind speed probability density functions for each season, for the years 2010-2015. (80 m)

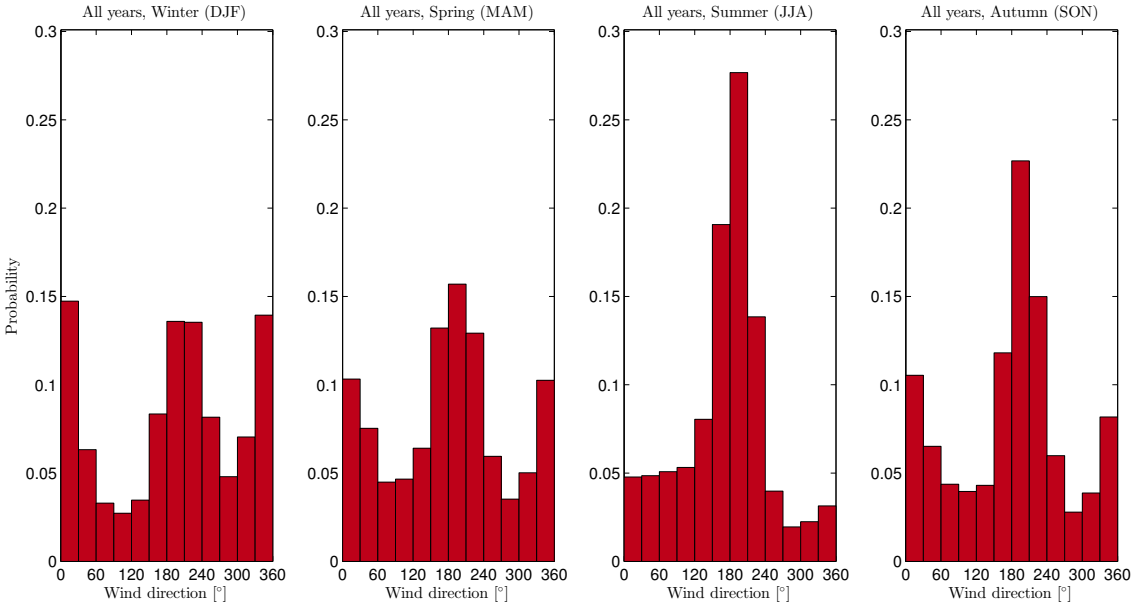

Figure 5: Wind direction probability density functions for each season, for the years 2010-2015.

The observations were divided by season and direction in 30° sectors in order to understand the variability and find the prevailing wind direction. For each season and sector, the average wind speed at

each height of 80, 90, 100, and 110 m was computed. Since we focus on the power available to a wind turbine, and power is dependent on u^3, the average wind speed was determined as $\sqrt[3]{\overline{u^3}}$. The data for each season and sector were then fitted to a power law profile using MATLAB. The parameters related to the power law profile are shown below in Figure 6.

	Hellman	z_r	$u(z_r)$
Winter	0.12	58	9.9
Spring	0.22	51	10.5
Summer	0.24	64	9.9
Autumn	0.22	55	10.1

Figure 6: Wind speeds are consistent throughout the year at the site. However, the wind speed gradient $\frac{\partial u}{\partial z}$ is less during winter.

Diurnal variations in wind speed and direction were also analyzed by constructing a wind rose for each hour of the day. While small variations in wind direction were observed, no significant diurnal variation appears to exist at the site. In general, the dominant wind direction only changes by about 30° throughout the day. The wind rose change throughout the day is shown in Figure 21 in the Appendix.

Once seasonal wind profiles were developed using data from the prevailing wind directions, our optimization model was run for each season. The model returns the optimal hub height for the given input array, and compares the power generated by this arrangement to two base cases ($h_{\text{hub}} = 100m$ and $h_{\text{hub}} = 200m$). An example solution for the 1-D model (i.e., a case where each turbine is behind another) is shown below.

$$U_\infty \Rightarrow (200m - 94m - 200m - 92m - 200m)$$

In practice, the small variations in optimal heights would be rounded, for the sake of construction feasibility. The two base cases are shown below.

$$U_\infty \Rightarrow (100m - 100m - 100m)$$

$$U_\infty \Rightarrow (200m - 200m - 200m)$$

Finally, we compare our optimized power output to an idealized condition where no wake effects are present (i.e., using the incoming velocity).

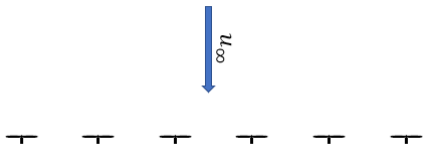

Figure 7: Wind direction probability density functions for each season, for the years 2010-2015.

3.1 Assumptions

For a given turbine, our optimization method only considers the wakes of its direct, upstream neighbors. That is, the deficit that the third row turbine feels is simply the sum of the deficits caused by turbines in rows 1 and 2. We also ignore the wake generated by the turbine towers for simplicity.

Our paper also assumes that, since the diurnal variations are small throughout the year, as previously discussed, the prevailing wind direction is either 180° or 360°; since our model considers a square array, only a small subset of inflow wind directions need to be considered. This range of wind directions is shown in Figure 8. Likewise, our paper assumes that the wind direction at a given time is constant at all heights.

The wake growth rate was calculated using a thrust coefficient of 0.5. This value was provided in lecture. The model used assumes wake grows symmetrically in the y and z directions. With thermal stratification and spatial variations in turbulence intensity, we expect that the wake will likely grow asymmetrically.

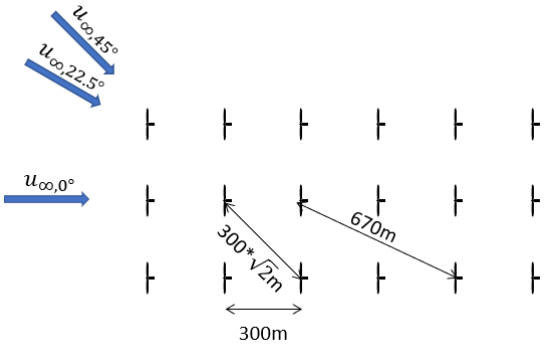

Figure 8: Due to the symmetry of the wind farm model, other angles need not be considered. The relevant turbine spacing for each scenario is also shown.

4 Analytical Model

The analytical model of Bastankhah and Porté-Agel (2014) is extended here to estimate the velocity deficit in a wind farm with turbines of varying hub heights. Drawing motivation from Lissaman (1979) and from pollutant dispersion problems covered in CEE 262B, we consider the velocity deficit within the wind farm to be well approximated as a simple linear superposition of wakes behind each individual turbine. Using Equation (1) as the building block, we define the normalized velocity deficit within the wind farm as follows:

$$C(x; x_{\text{hub},i}) = \left(1 - \sqrt{1 - \frac{C_T}{8(k_w(x - x_{\text{hub},i})/d_0 + \epsilon)^2}}\right), \tag{3}$$

$$S(x, y, z; x_{\text{hub},i}, y_{\text{hub},i}, z_{\text{hub},i}) = \exp\left(- \frac{1}{2(k_w(x - x_{\text{hub},i})/d_0 + \epsilon)^2} \left\{ \left(\frac{z - z_{\text{hub},i}}{d_0}\right)^2 + \left(\frac{y - y_{\text{hub},i}}{d_0}\right)^2 \right\}\right), \tag{4}$$

$$I(x, y, z; x_{\text{hub},i}, y_{\text{hub},i}, z_{\text{hub},i}) = \exp\left(- \frac{1}{2(k_w(x - x_{\text{hub},i})/d_0 + \epsilon)^2} \left\{ \left(\frac{z + z_{\text{hub},i}}{d_0}\right)^2 + \left(\frac{y + y_{\text{hub},i}}{d_0}\right)^2 \right\}\right), \tag{5}$$

$$\frac{\Delta U}{U_\infty} = \sum_{i=1}^{n} C_i \times (S_i + I_i), \tag{6}$$

where C_i is the maximum velocity deficit for turbine i, S_i represents the radially spreading velocity deficit for turbine i, and I_i represents an image of the velocity deficit required to satisfy the no-flux boundary condition at $z = 0$ m. The velocity deficit for a simple test case involving a single row of wind turbines with two different turbine hub heights ($z_{\text{hub}} = 100$ m and $z_{\text{hub}} = 150$ m) is shown in Figure 9.

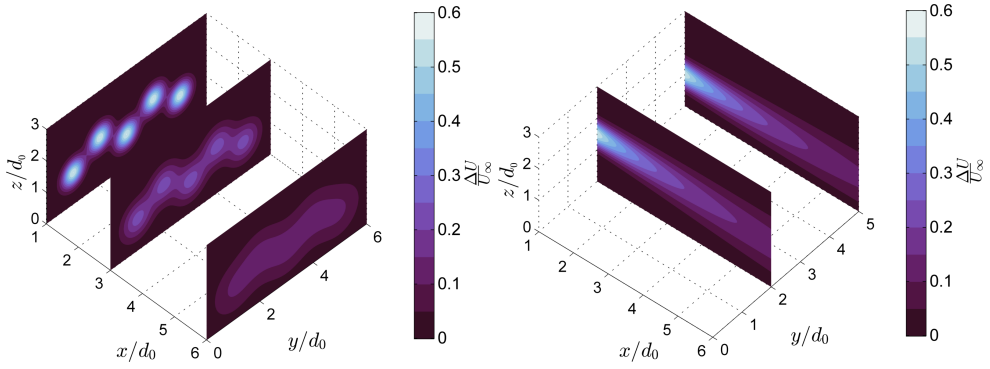

Figure 9: 2-D maps of the normalized velocity deficit as a function of normalized spatial distances x/d_0, y/d_0, and z/d_0. The wake behind a single row of turbines with two turbines rotor heights (tall with $z_{\text{hub}} = 150$ m, and small with $z_{\text{hub}} = 100$ m).

5 Optimization Problem

The following section describes the condensed form of the 2-D optimization problem that was used in this paper. The optimization problem was run using the LGO solver in JuMP (Mathematical Optimization module in Julia programming language).

5.1 Parameters

$h_{min} = 70m$, $h_{max} = 200m$, $C_P = 0.3$, $d_0 = 100m$, $\rho = 1.07\frac{kg}{m^3}$, $i = rows \in 1, ..., 3$, $j = cols \in 1, ..., 3$, $k_w = 0.06$, $\epsilon = 0.22$, $C_T = 0.5$

5.2 Objective

Maximize power output from wind farm for a given inflow wind $u(z)$

$max : f(x) = \sum_{i=1}^{N} P_i$

5.3 Decision Variables

$h_{hub}^{i,j}$: variable for hub height [m] of each turbine in the wind farm (i rows, j cols)

5.4 Constraints

$\forall i, j : h_{min} \leq h_{hub}^{i,j} \leq h_{max}$

5.5 Expressions

The following velocity deficit equations are adapted from Bastankhah and Porté-Agel (2014).

$$v_{deficit}^{i,j}(y,z) = C1_{i,j} + \exp\left(C2_{i,j} * C3_{i,j}(y,z)\right)$$

where:

$$C1_{i,j} = 1 - \sqrt{1 - \frac{C_T}{8(k_w(x_i - x_{i-1})/d_0 + \epsilon)^2}}$$

$$C2_{i,j} = -\frac{1}{2(k_w(x_i - x_{i-1})/d_0 + \epsilon)^2}$$

$$C3_{i,j}(y,z) = \left(\frac{z - h_{hub,i-1,j}}{d_0}\right)^2 + \left(\frac{y - y_{hub,i-1,j}}{d_0}\right)^2$$

(affected only by closest turbine in previous row)

$$v_{wake}^{i,j}(y,z) = (1 - v_{deficit}^{i,j}) * u_\infty(z)$$

$$region_{extracted}^{i,j} = \left[(y - y_{hub}^{i,j})^2 + (z - z_{hub}^{i,j})^2\right] \leq \left(\frac{d_0}{2}\right)^2$$

(calculates the region within the swept area of turbine (i, j))

$$v_{extracted}^{i,j} = region_{extracted}^{i,j} * v_{wake}^{i,j}$$

(calculates the wake velocity in the swept region of turbine (i, j))

$$v_{extracted,cubed}^{i,j} = \left(v_{extracted}^{i,j}\right)^3$$

(cube each individual wake velocity element within the swept area - this value will is proportional to P_i, since the other parameters are held constant.)

6 Results

6.1 Comparison with Base Case (1-D)

Model runs were performed for a 1-D version of our model with 8 turbines, where each turbine is directly behind the prior turbine. This is our *worst case* scenario. The optimized power outputs for each a value are then compared to a case where every turbine was 100m or 200m tall, respectively. The model was run for the three turbine distances mentioned in our *Approach* section. The results of this analysis are presented below in Figures 10, 11, and 12.

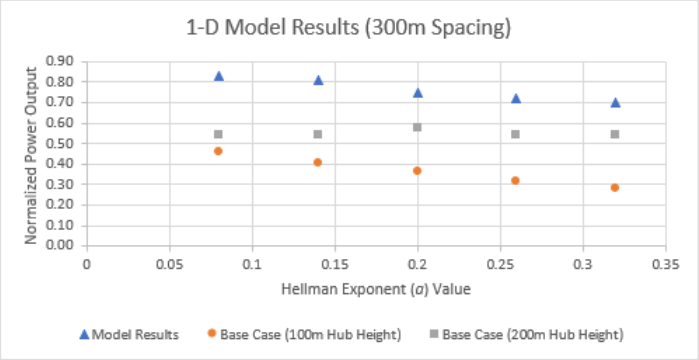

Figure 10: Normalized power values. The optimized hub heights outperform the base cases for all a values.

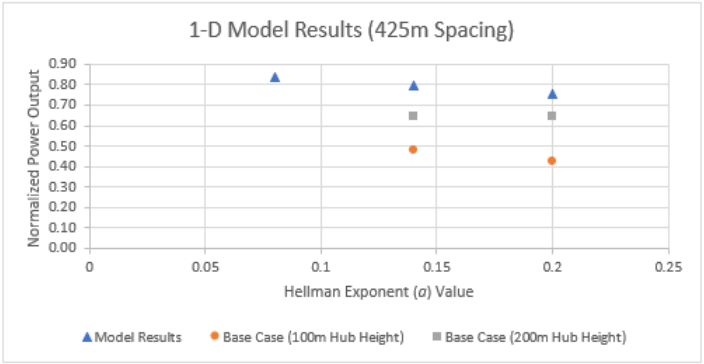

Figure 11: The normalized optimal power value is consistent for different turbine spacing distances.

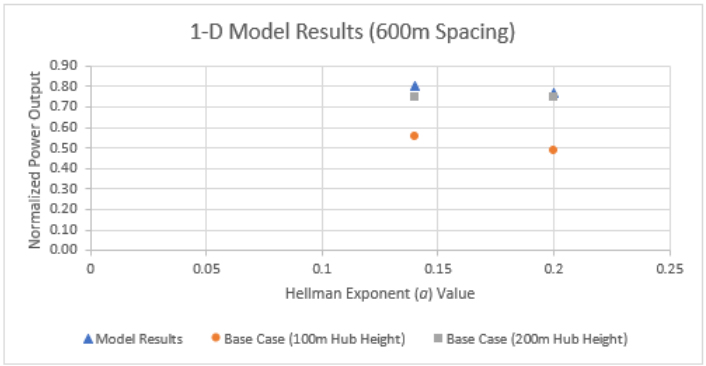

Figure 12: As the spacing distances increase, the optimal solution and the 200m base case converge.

The values in Figures 10, 11, and 12 are normalized by the power output from the best-case scenario. In the best-case scenario, the wind blows perpendicular to the row of turbines with all turbines with a hub height of 200 m. The base case power outputs consisted of a row of turbines that were all the same height. For the worst-case scenario, the optimized hub heights improve power output by 28% for high a values, to 53% for low a values, compared to the base case.

A table of all the power calculations is shown in the Appendix.

6.2 Comparison with Base Case (2-D)

The model was also used to calculate the normalized power for a 2-D wind farm. The model wind farm was 3 rows by 3 columns, with equal spacing in both directions. A 2-D model was developed in order to produce more realistic power results. The resulting velocity deficit contours for each row are shown below in Figures 13 and 14.

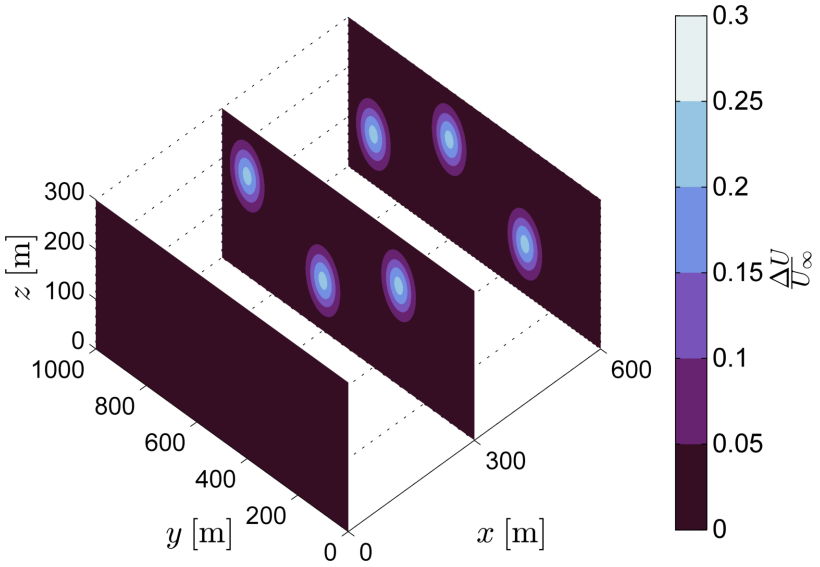

Figure 13: The first row does not experience a velocity deficit. Subsequent rows experience a deficit according to the location of the previous turbine.

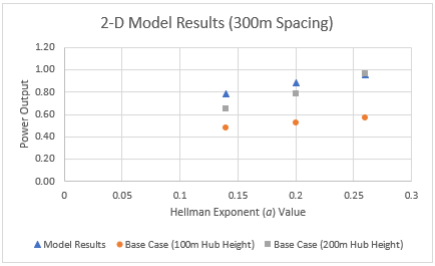

Figure 14: For the 2-D case, the values for the base case converge with the optimal solution more quickly.

The 2-D solution quality was limited by computing power. Since the entire width of each turbine row had to be considered for the optimization problem, grid resolution was limited to 2 m by 2 m. An interesting takeaway is that the normalized power outputs are higher for the 2-D case than for the 1-D case. This can be explained by the fact that in 2-D, a larger proportion of the turbines are experiencing the original/unmodified inflow velocity. Higher normalized power outputs corresponds to less need for varying hub heights.

6.3 Comparison with Base Case (2-D) - Flexible Y position

To verify the model performance, the constraint on the y-position of each turbine in the second and third rows was removed. However, a maximum y-position and minimum spacing requirements were maintained. As expected, the model converged on a solution with staggered y-positions for the worst-case scenario. An example of this solution is shown below in Figure 15.

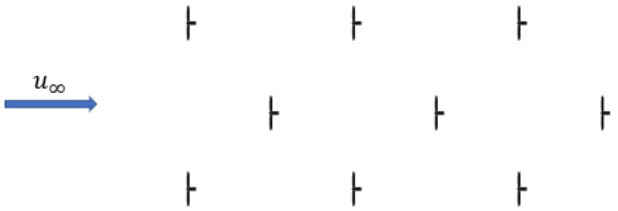

Figure 15: The model moved the lone turbines into the space between the previous row's turbines, in order to minimize the velocity deficit experienced by both itself and the following row.

7 Sensitivity Analysis

The following sections describe various factors that affect the results of the optimization model.

7.1 Hellman Exponent

Our model is sensitive to variations of the Hellman exponent. We found that, with increasing a, the model begins to place all turbines at the highest height possible. This is because, with increasing a, $\frac{\partial u}{\partial z}$ is larger, and thus losses due to overlapping wakes become less important than the wind speed gains with increased height. Three velocity profiles with different values of a (estimated from the observations from Texas) are shown in Figure 16.

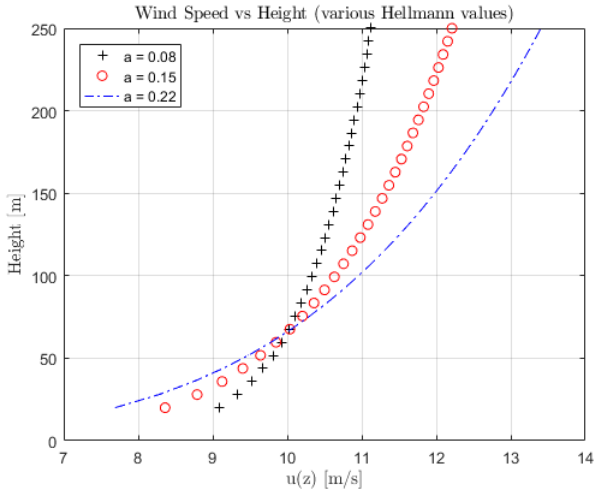

Figure 16: Higher a values lead to a higher velocity gradient

Figure 17 shows 2-D velocity fields 300 m behind a single turbine for two different Hellman values ($a = 0.08$ and $a = 0.22$).

7.2 Varying Wind Angle

Due to the symmetry of our 2-D model, all possible wind cases can be modeled by varying the inflow wind direction from 0 to 45°. To model various angles, the spacing between turbines in both directions was scaled appropriately. For example, for the 45° case, the spacing between turbines was changed from 300m to $300\sqrt{2}$m. A table of power generation versus wind angle is shown in Figure 18.

The hourly wind directions could be considered in the future in order to better estimate the annual power output of a wind farm with varying turbine hub heights.

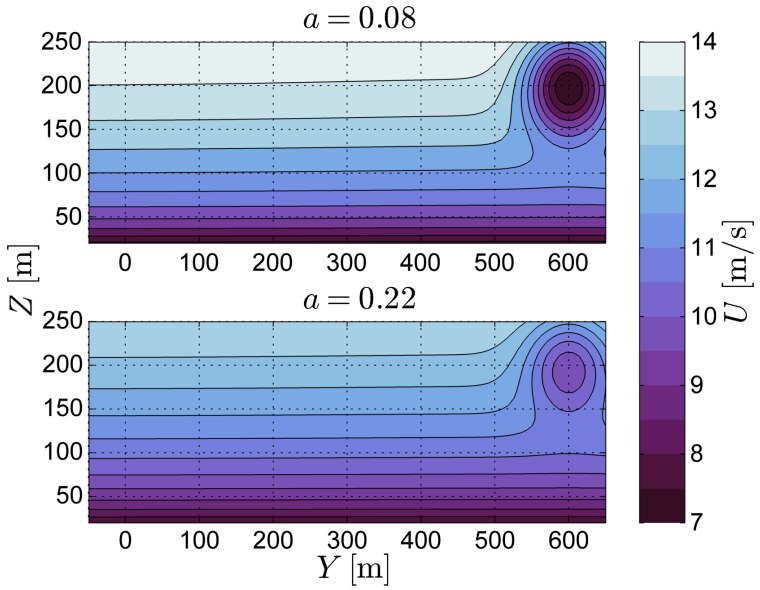

Figure 17: With an a value of 0.08, the wake velocity is formed such that lowering the hub height increases the power output. With an a value of 0.22, the wake does not impact the optimal hub height.

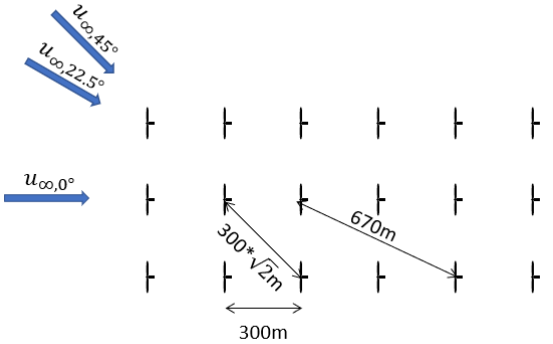

Figure 18: For a wind farm with 300m spacing and 100m rotor diameter, the furthest a wake can travel unimpeded is two rows.

8 Conclusion

For the 1-D case, it is advantageous to modify the hub heights of the turbines for all Hellman exponent values when the turbine spacing is 300 m. As the turbine spacing increases, the model's optimal solution converges to the 200 m base case solution. This occurs at a turbine spacing of approximately 600 m. This demonstrates that, for high spacing distances, it is optimal to make every turbine as tall as possible, even if they are often within another turbine's wake.

As engineers aim to maximize wind power generation per unit surface area, work on optimal turbine placement will continue, and increased computing capabilities will allow for new and more accurate turbine siting algorithms.

8.1 Next Steps

Future research should examine the power generation for each day separately. This research should also examine the full range of wind directions instead of just focusing on the dominant wind directions. Furthermore, the variability of energy prices could be considered as well with the goal of maximizing power production especially during operational times when electricity prices are high. In the case of Texas, this likely includes summer months, when cooling loads increase.

Our model does not consider the wake generated by the turbine towers. In the case where the next turbine is placed at a lower height than a upstream turbine, the velocity deficit caused by the wake of the upstream tower may alter the results of the optimization model and lead to a solution with all turbine hub heights being set to high as possible.

Furthermore, effects of thermal stratification and spatially varying turbulence intensity are not considered. Stable stratification could inhibit the spreading of the velocity deficit, which was modeled as a passive scalar. A modified log-law velocity profile correcting for weak thermal stratification could also be used to calculate the incoming wind. Increased turbulence intensity may lead to a more rapid wake growth since the analytical velocity deficit model involves a variance which would scale like the eddy viscosities. We expect that the wake could grow asymmetrically due to thermal stratification and spatial gradients in turbulence intensity.

Finally, it would be advantageous to run a model that determines the optimal horizontal location (x, y) of each turbine. This will require a higher-resolution mesh, and therefore, a more powerful computer.

9 Appendix

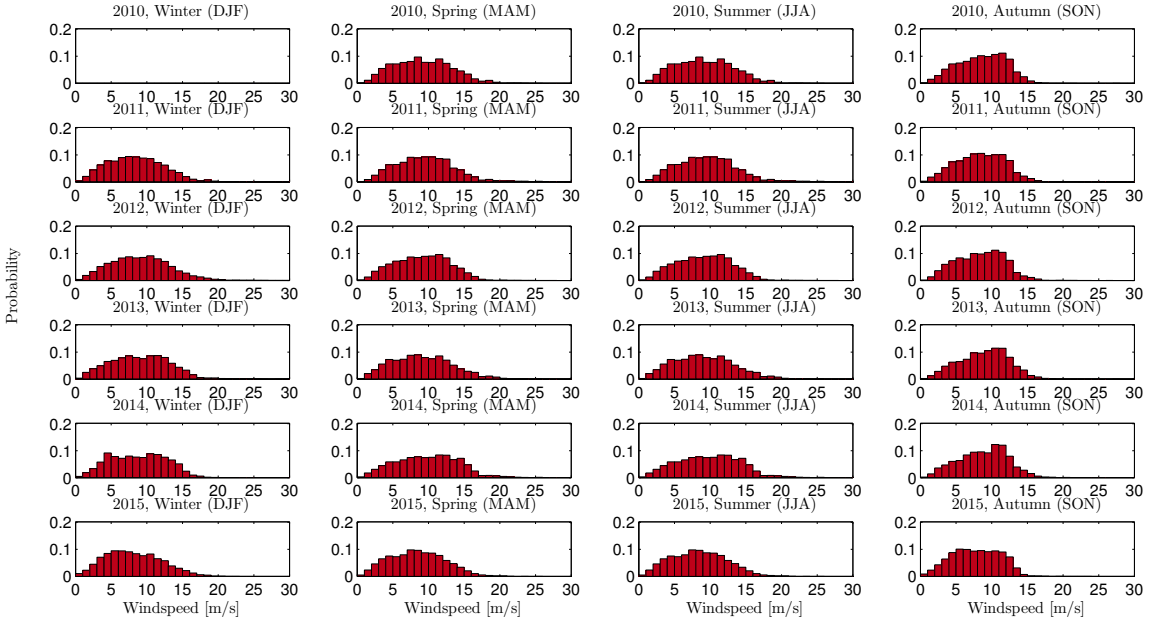

Figure 19: Wind speed probability density functions for each season, for each year.

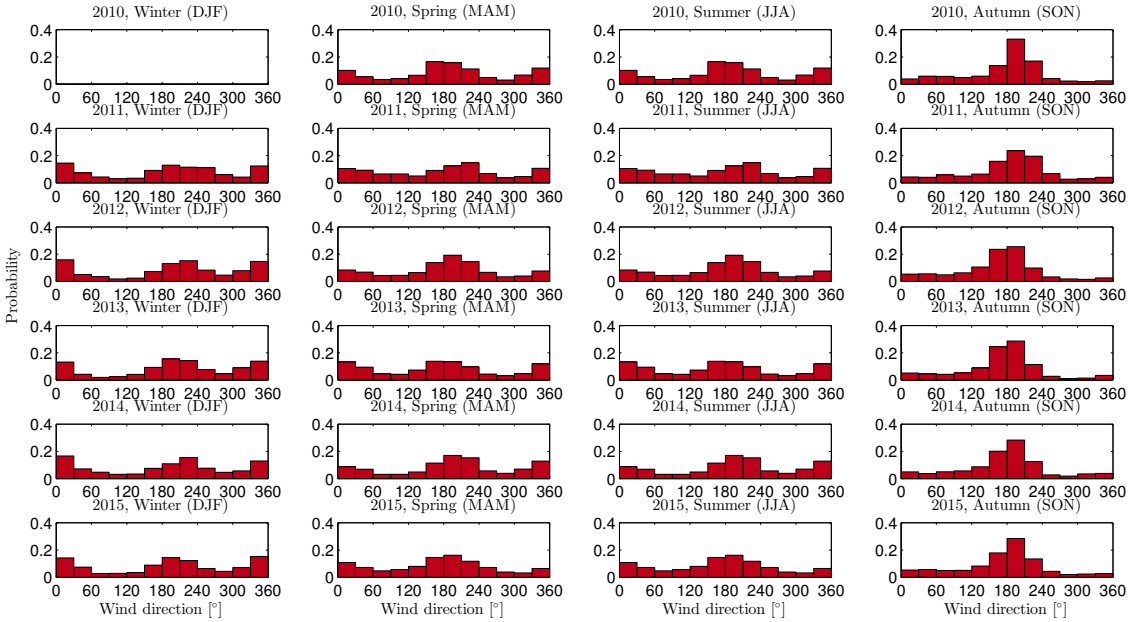

Figure 20: Wind direction probability density functions for each season, for each year.

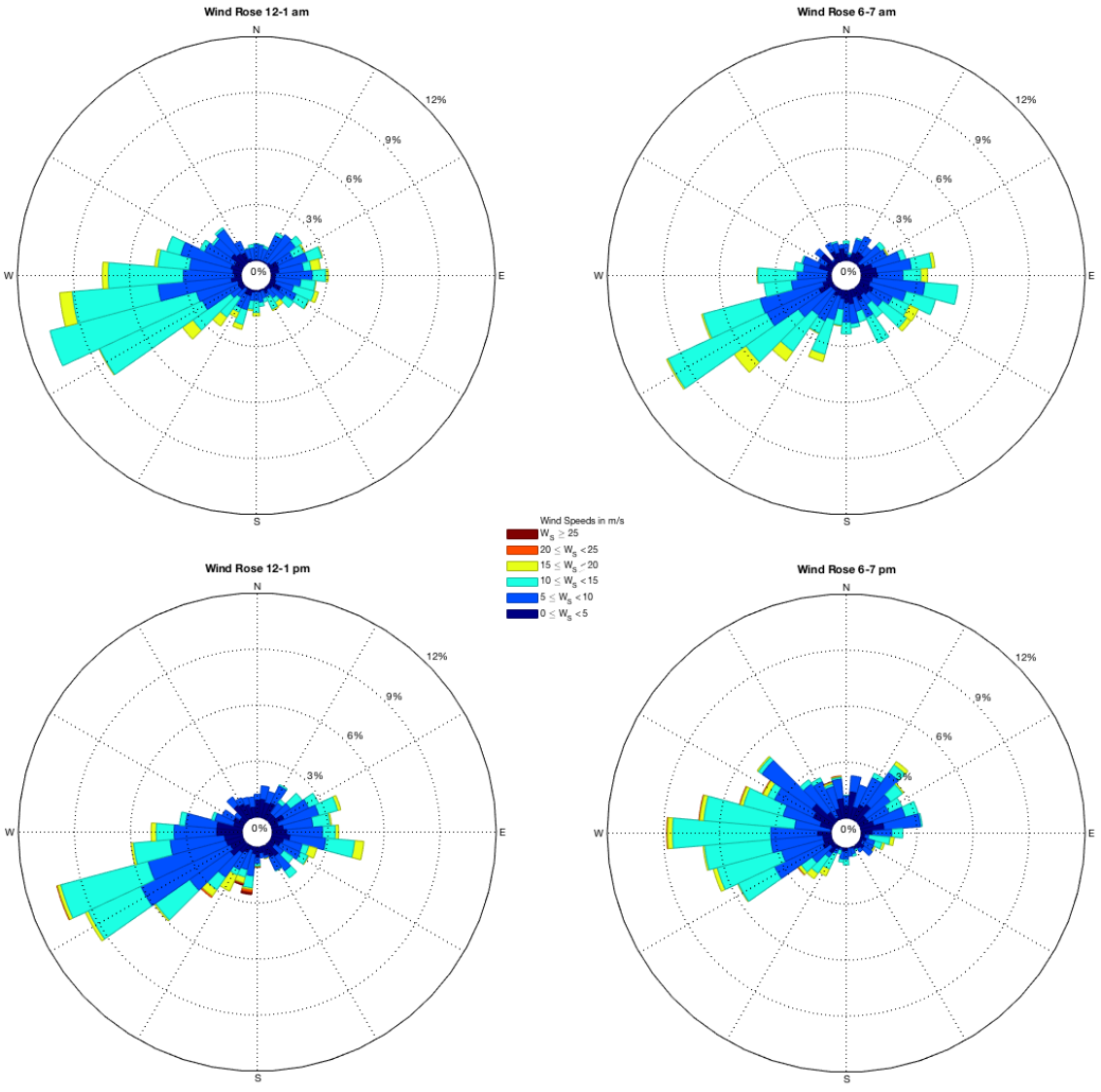

Figure 21: Wind rose change throughout the day. (80 m)

1D Model Data

Run #	σ value	z_r	# turbines (not including first 2)	X-Spacing	Y-mesh (# pts)	Z-mesh (#pts)	Objective Value	Improvement From Base (100m)	Improvement From Base (200m)	Objective (Normalized by 200m optimal case)	
1	0.08	66.77	8	300	50	100	1.40E+07	81.92%	53.48%	0.83	
2	0.14	66.77	8	300	50	100	1.66E+07	100.97%	49.40%	0.81	
3	0.2	66.77	8	300	50	100	1.87E+07	105.46%	29.39%	0.75	
4	0.26	66.77	8	300	50	100	2.19E+07	129.08%	32.93%	0.72	
5	0.32	66.77	8	300	50	100	2.58E+07	150.11%	28.54%	0.70	
Base100	0.08	66.77	8	300	50	100	7.70E+06	---	---	0.46	
Base100	0.14	66.77	8	300	50	100	8.26E+06	---	---	0.40	
Base100	0.2	66.77	8	300	50	100	9.10E+06	---	---	0.36	
Base100	0.26	66.77	8	300	50	100	9.57E+06	---	---	0.31	
Base100	0.32	66.77	8	300	50	100	1.03E+07	---	---	0.28	
Base200	0.08	66.77	8	300	50	100	9.12E+06	---	---	0.54	
Base200	0.14	66.77	8	300	50	100	1.11E+07	---	---	0.54	
Base200	0.2	66.77	8	300	50	100	1.45E+07	---	---	0.58	
Base200	0.26	66.77	8	300	50	100	1.65E+07	---	---	0.54	
Base200	0.32	66.77	8	300	50	100	2.01E+07	---	---	0.54	
6	0.08	66.77	8	424.26	50	100	1.41E+07	---	---	0.84	
7	0.14	66.77	8	424.26	50	100	1.64E+07	66.71%	23.95%	0.80	
8	0.2	66.77	8	424.26	50	100	1.88E+07	78.34%	17.05%	0.75	
Base 100	0.14	66.77	8	424.26	50	100	9.82E+06	---	---	0.48	
Base 100	0.2	66.77	8	424.26	50	100	1.06E+07	---	---	0.42	
Base 200	0.14	66.77	8	424.26	50	100	1.32E+07	---	---	0.64	
Base 200	0.2	66.77	8	424.26	50	100	1.61E+07	---	---	0.64	
9	0.14	66.77	8	600	50	100	1.64E+07	44.20%	7.22%	0.80	
10	0.2	66.77	8	600	50	100	1.92E+07	56.86%	2.96%	0.77	
Base 100	0.14	66.77	8	600	50	100	1.14E+07	---	---	0.55	
Base 100	0.2	66.77	8	600	50	100	1.22E+07	---	---	0.49	
Base 200	0.14	66.77	8	600	50	100	1.53E+07	---	---	0.75	
Base 200	0.2	66.77	8	600	50	100	1.86E+07	---	---	0.75	

Orthogonal Wind Case (i.e. no wake)							Objective Value	Improvement From Base Worst Case (300m spacing)	Improvement From Base Worst Case (424m spacing)	Improvement From Base Worst Case (600m spacing)	Improvement From Optimized Worst Case (300m spacing)
Hub Height											
Base 100	0.14	66.77	8	N/A	50	100	1.52E+07	84.57%	55.13%	34.14%	-8.16%
Base 100	0.2	66.77	8	N/A	50	100	1.64E+07	80.07%	55.13%	34.14%	-12.36%
Base 200	0.08	66.77	8	N/A	50	100	1.68E+07	---	---	---	20.22%
Base 200	0.14	66.77	8	N/A	50	100	2.05E+07	84.52%	55.11%	34.14%	23.50%
Base 200	0.2	66.77	8	N/A	50	100	2.50E+07	72.76%	55.11%	34.14%	33.52%
Base 200	0.26	66.77	8	N/A	50	100	3.04E+07	84.52%	---	---	38.81%
Base 200	0.32	66.77	8	N/A	50	100	3.71E+07	84.52%	---	---	43.54%

Figure 22: The normalized optimal power value is consistent for different turbine spacing distances.

2D Model Data

Run #	a value	z_r	# turbines (not including "imaginary" rows)	X-Spacing	Y-mesh (# pts)	Z-mesh (#pts)	Objective Value	Improvement From Base (100m)	Improvement From Base (200m)
1	0.14	66.77	9	300	100	40	2.37E+06	63.25%	21.81%
2	0.2	66.77	9	300	100	40	2.65E+06	70.26%	12.19%
3	0.26	66.77	9	300	100	40	2.88E+06	69.41%	-0.12%
Base100	0.14	66.77	9	300	100	40	1.45E+06	---	---
Base100	0.2	66.77	9	300	100	40	1.56E+06	---	---
Base100	0.26	66.77	9	300	100	40	1.70E+06	---	---
Base200	0.14	66.77	9	300	100	40	1.94E+06	---	---
Base200	0.2	66.77	9	300	50	100	2.37E+06	---	---
Base200	0.26	66.77	9	300	50	100	2.88E+06		

Figure 23: The normalized optimal power value is consistent for different turbine spacing distances.